

Relaxation Time Constants and Apparent Diffusion Coefficients of Rat Retina at 7 Tesla

Govind Nair,¹ Qiang Shen,² Timothy Q. Duong^{2,3}

¹ Graduate School of Biomedical Science, University of Massachusetts Medical School and Worcester Polytechnic Institute, MA

² Departments of Ophthalmology, Radiology and Physiology, Research Imaging Institute, University of Texas Health Science Center, San Antonio, TX

³ Department of Veterans Affairs, South Texas Veterans Health Care System, San Antonio, TX

Received 25 March 2010; accepted 2 April 2010

ABSTRACT: MRI has recently been applied to study the retina *in vivo*. Measurements of relaxation time constants (T_1 , T_2 , and T_2^*) and the apparent diffusion coefficient (ADC) of the retina would be useful to systematically optimize structural, physiological, and functional MRI contrasts. MRI studies were performed on 12 anesthetized and paralyzed rats. High-resolution T_1 , T_2 , T_2^* and ADC of the rat eyes were measured at $50 \times 50 \times 800 \mu\text{m}$ at 7 Tesla. Profiles of T_1 , T_2 , T_2^* and ADC across the retinal thickness were analyzed. Region of interests of three layers across the retinal thickness were tabulated. This study demonstrated that high resolution T_1 , T_2 , T_2^* and ADC of the rat retina could be imaged. Profile analysis of T_1 , T_2 , T_2^* and ADC across the retinal thickness were helpful to minimize partial volume effects. T_1 , T_2 , T_2^* and ADC of the rat retina were overall similar to those of the brain. Quantitative T_1 , T_2 , T_2^* and ADC may change in retinal diseases and their measurements could help to stage retinal disease progression and monitor therapeutic intervention. © 2010 Wiley Periodicals, Inc. *Int J Imaging Syst Technol*, 20, 126–130, 2010; Published online in Wiley InterScience (www.interscience.wiley.com). DOI 10.1002/ima.20237

Key words: spin–spin relaxation time; spin-lattice relaxation time; BOLD; brain; apparent diffusion coefficient; eye

I. INTRODUCTION

Rats are good experimental models for a wide range of retinal diseases, including retinitis pigmentosa, diabetic retinopathy, glaucoma, and macular degeneration because retinal layouts are similar across many mammalian species. The retina has historically been imaged using optical techniques. Fundus camera provides surface anatomy and optical coherence tomography offers depth-resolved anatomy (Fujimoto et al., 2000). Fluorescein angiography (Preussner et al., 1983), indocyanin-green angiography (Guyer et al., 1993), laser

speckle imaging (Cheng et al., 2007), and laser Doppler flowmetry (Riva et al., 1994) have been applied to measure relative blood flow or blood velocity. Intrinsic optical imaging provides relative oxygenation and blood volume (Nelson et al., 2005). While these optical imaging techniques have made remarkable contributions to our understanding of retinal anatomy, physiology and function, they require an unobstructed pathway of light for signal detection. Diseases such as senile cataract formation and some vitreal hemorrhage may preclude the use of optically based imaging techniques.

Magnetic resonance imaging is a noninvasive diagnostic tool that provides anatomical, physiological (oxygenation, blood flow, and blood volume), and functional information in a single setting. While MRI has lower spatial resolution and longer acquisition time compared to optical imaging techniques, MRI provides a large field of view without depth limitation and is not limited by opacity of the media. Advances in MRI technologies contributed by numerous laboratories have made possible very high spatial resolution capable of visualizing columnar (Duong et al., 2001; Kim et al., 2000; Cheng et al., 2001) and laminar structures (Silva et al., 2002) of the brain *in vivo*. MRI of the retina requires substantially higher spatial resolution and a few high-resolution MRI studies of the retina in animal models have been reported. These include layer-specific anatomical (Cheng et al., 2006; Shen et al., 2006), basal blood-flow and physiologically induced blood-flow (Li et al., 2008) MRI, visually evoked (Duong et al., 2002) and layer-specific, physiologically induced BOLD fMRI (Chen et al., 2008).

Measurements of relaxation time constants (T_1 , T_2 , and T_2^*) and the apparent diffusion coefficient (ADC) of the retina would help lay a foundation for future studies and would be useful to optimize structural, physiological and functional MRI contrasts. These MRI parameters may change in retinal diseases and could help to stage retinal disease progression and monitor therapeutic intervention. Measurements of relaxation time constants and ADC have been reported in the cat retina at 4.7 Tesla (Shen et al., 2006) and mouse retina at 11.7

Correspondence to: Timothy Duong; e-mail: duongt@uthscsa.edu
Grant sponsors: This work was supported by NIH/NEI (R01EY014211, R01EY018855) and VA MERIT to T.Q.D.

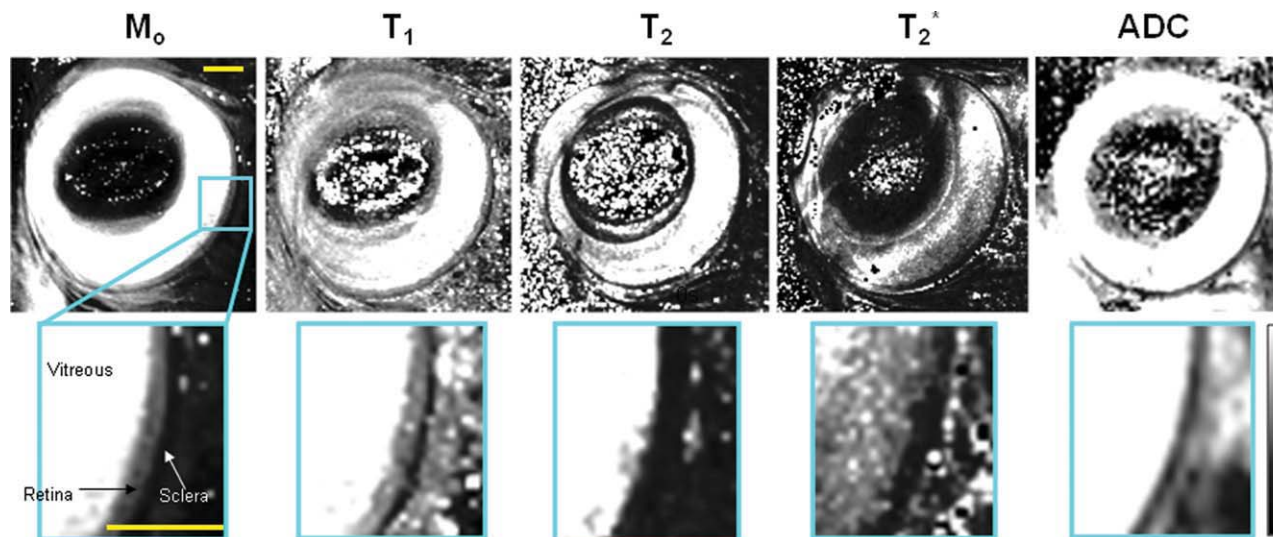


Figure 1. Representative M_0 (from T_1 data), T_1 , T_2 , T_2^* and ADC maps of a rat eye at $50 \times 50 \times 800 \mu\text{m}$. The yellow scale bar is 1 mm. The grayscale bar indicates 0–4 s for T_1 , 0–200 ms for T_2 , 0–50 ms for T_2^* and $0\text{--}2 \times 10^{-3} \text{ mm}^2/\text{s}$ for ADC. [Color figure can be viewed in the online issue, which is available at www.interscience.wiley.com.]

T (Chen et al., 2008). This study reports quantitative T_1 , T_2 , T_2^* and ADC in the rat retina at 7 T, a field strength that is more widely available.

II. METHODS

A. Animal Preparations. Twelve normal adult male Sprague Dawley rats (350–400 g) were studied, where T_1 , T_2 and ADC were measured on five animals, and T_2^* were measured on four animals (multiple parameters were measured in some rats). Animals were anesthetized with 1.1% isoflurane, paralyzed with pancuronium bromide (3 mg/kg first dose, 1 mg/kg/h, ip), and mechanically ventilated during MRI as described previously (Cheng et al., 2006; Li et al., 2008). End-tidal CO_2 (Surgivet capnometer), heart rate and arterial oxygen saturation (Nonin-8600, Plymouth, MN), and rectal temperature (Digisense, Cole Palmer) were monitored and maintained within normal physiological ranges. Noninvasive end-tidal CO_2 values were previously calibrated against invasive blood-gas samplings under identical setting. Invasive blood-gas sampling was not performed. This animal preparation protocol has been shown to yield highly stable MRI data over long acquisition time (Duong and Muir, 2009; Cheng et al., 2006; Li et al., 2008). Cornea was kept moist during the study using methylcellulose.

B. MRI Methods. MRI studies were performed on a 7-Tesla/30-cm magnet and a 40G/cm B-GA12 gradient insert (Bruker, Billerica, MA). Rats were placed in a head holder consisting of ear and tooth bars. A small circular surface coil (ID~7 mm) was placed on the left eye. Magnetic field homogeneity was optimized using standard FASTMAP shimming with an isotropic shimming voxel encompassing the entire eye. MRI hardware and animal stability have been evaluated and optimized to yield highly stable MRI data over long acquisition time (Duong et al., 2009).

A single mid-sagittal imaging slice bisecting the center of the eye was imaged to minimize partial-volume effect due to retinal curvature (Cheng et al., 2006; Li et al., 2008). For T_1 , T_2 and T_2^* measurements, FOV = $12.8 \times 12.8 \text{ mm}$, matrix = 256×256 . For ADC measurements, FOV = $6.4 \times 6.4 \text{ mm}$, matrix = 128×128 . All have the same spatial resolution of $50 \times 50 \times 800 \mu\text{m}$.

T_1 was measured using saturation recovery technique with 8-segment, spin-echo EPI, TE = 31.1 ms, variable TR = 100, 200, 400, 800, 1600, 3200, and 6400 ms (90° flip angle), and number of transient (NT) = 16 (58 min). T_2 was measured using spin-echo EPI with TR = 2000 ms (90° flip angle), variable TE = 31, 41, 51, 61, 81, and 101 ms, and NT = 16 (51 mins). T_2^* was measured using conventional gradient-echo with TR = 400 ms (40° flip angle), variable TE = 6.5, 12, 18 ms, and NT = 12 (61 mins). ADC was measured using conventional spin echo sequence with TR = 20 s (90° flip angle), $b = 0$ and 3 orthogonal diffusion directions in three separate scans with $b = 1000 \text{ s/mm}^2$, and NT = 4 (68 mins). All data were acquired without cardiac or respiratory gating. Although these measurements herein were long to maximize accuracy, future studies could use smaller number of arrayed parameters and not all relaxation time constants and ADC needed to be measured in a single setting.

We are cognizant of many other methods to measure relaxation time constants and ADC, these sequences and protocols were chosen given the high spatial resolution consideration and time constraint.

C. Data Analysis. Image analysis employed codes written in Matlab (MathWorks Inc., Natick, MA, USA) and STIMULATE software (University of Minnesota). Time-series images were coregistered if needed as described previously (Cheng et al., 2006). Quantitative T_1 , T_2 , T_2^* and ADC maps were calculated pixel-by-pixels using nonlinear least squared regression to single exponential functions. To minimize bias, the retina was first detected using an edge-detection technique and automated profile analysis was performed (Cheng et al., 2006) to derive T_1 , T_2 , T_2^* and ADC values across the retinal thickness. Radial projections perpendicular to the vitreous boundary were then obtained with ($3\times$) spatial interpolation. The retinal thicknesses were divided into three equal bands on the profiles and MRI parameters were tabulated and averaged. The choices of the three equal bands were based on previous reported of three roughly equal MRI-defined layers, cognizant of some partial volume effects (PVE) (Cheng et al., 2006). Reported values and error bars are in mean \pm SD. Statistical tests employed Student t -test with $P < 0.05$ indicating statistical significance.

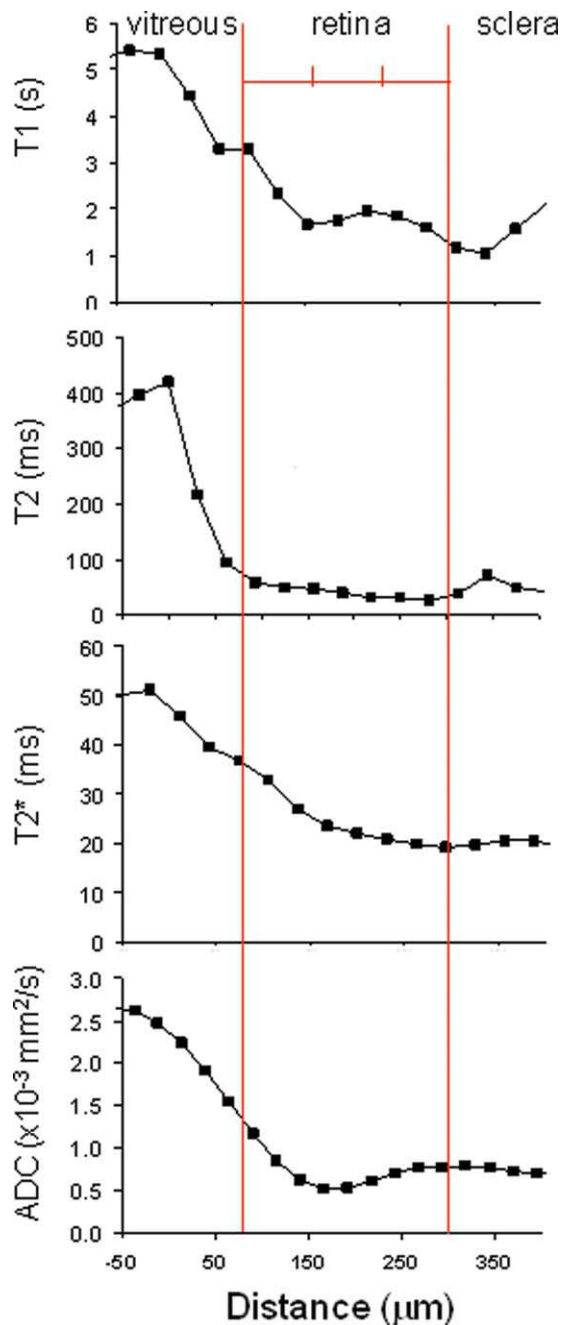


Figure 2. Profiles of T_1 , T_2 , T_2^* and ADC across the retinal thickness. [Color figure can be viewed in the online issue, which is available at www.interscience.wiley.com.]

III. RESULTS

Typical Mo (from T_1 data), T_1 , T_2 , T_2^* and ADC maps at $50 \times 50 \times 800 \mu\text{m}$ are shown in Figure 1. T_1 , T_2 , T_2^* and ADC of the more fluid-like vitreous were high compared to the retina. There were generally no apparent laminar contrasts within the retina on quantitative maps. To better visualize the spatial variation of the retina, T_1 , T_2 , T_2^* and ADC profiles across the retinal thickness are shown in Figure 2. Partial-volume effect was more substantial on the side of the retinal-vitreous boundary than the side of the retinal-scleral boundary which appeared negligible.

Figure 3 shows the group-averaged T_1 , T_2 , T_2^* and ADC values of three equal ROI's taken across the thickness of the retina. There

are approximately two to three pixels across the retinal thickness per ROI. Overall, most of these quantitative parameters were similar across the retinal thickness with a few exceptions with statistically different as shown.

Table I compares quantitative MRI parameters of the retina and vitreous of rat, mouse and cat. While there are differences in measurement parameters, field strengths, species, analysis and the extent of partial-volume effect, these quantitative MRI parameters are generally consistent across different groups.

IV. DISCUSSION

This study reports quantitative T_1 , T_2 , T_2^* and ADC of the retina across the retinal thickness at 7 T. These measurements are challenging. Animal and hardware stabilities are critical. By plotting profiles across the retinal thickness, potential partial-volume effects could be visualized. Whole-retina T_1 , T_2 , T_2^* and ADC were reliably determined and their values were overall similar to those of the brain, but were smaller than those of the vitreous as expected. These quantitative data could help to systemically optimize structural, physiological and functional MRI contrasts in the retina. T_1 , T_2 , T_2^* and ADC may also prove useful to stage retinal disease progression and monitor therapeutic intervention.

MRI quantitative maps and profiles did not show consistent laminar structure, in contrast to previously reported T_1 -/ T_2 - and diffusion-weighted images (Cheng et al., 2006; Shen et al., 2006) and at higher field (Chen et al., 2008). The lack of laminar resolution is unlikely due to eye movement or scanner instability in our measurements (Cheng et al., 2006; Li et al., 2008). Possible explanations are: (1) High temporal resolution EPI readout herein might have some spatial blurry compared to the previous reports employed conventional data acquisition techniques (Cheng et al., 2006; Shen et al., 2006; Chen et al., 2008). Such blurring is difficult to determine in practice. Nonetheless MRI parameters measured with EPI readout are also relevant. (2) Quantitative maps could have smaller dynamic ranges than weighted images. (3) Higher field, such as 11.7 T, could yield better contrasts among retinal layers. (4) There could be different extent of partial-volume effects arising from species differences and/or spatial resolution. Further studies are needed to clarify these potentially contributing factors.

A. T_1 . Rat vitreous and whole-retina T_1 values were, respectively, 4.6 ± 0.5 s and 2.5 ± 0.7 s at 7 T. The profile plots showed T_1 of the retina was likely overestimated due to PVE with the vitreous which has very long T_1 . Indeed, T_1 of middle and outer bands of the retina was ~ 1.8 s. A previous study in mice at 11.7 T using conventional data acquisition reported vitreous and retina T_1 of 4.2 and 2.5 s, respectively (Chen et al., 2008). Surprisingly, the vitreous T_1 at 7 T and 11.7 T were similar given that the T_1 should increase with field strength. This minor discrepancy could be due to different imaging parameters. By comparison, rat brain T_1 is 1.6–1.8 s at 7 T (Guilfoyle et al., 2003; Barbier et al., 2005).

B. T_2 . Rat vitreous and whole-retina T_2 values were, respectively, 420 ± 40 ms and 43 ± 9 ms at 7 T. A previous study in cat at 4.7 T using fast spin-echo acquisition reported vitreous T_2 of 218 (Shen et al., 2006), and in the inner, middle and outer bands of the cat retina at 4.7 T were 67 ± 5 , 48 ± 5 and 95 ± 6 ms, respectively. The inner band value was large because of potential PVE with the vitreous. Another study in mice at 11.7 T reported vitreous and retina T_2 of 70 ms and 25 ms, respectively, using conventional spin-echo

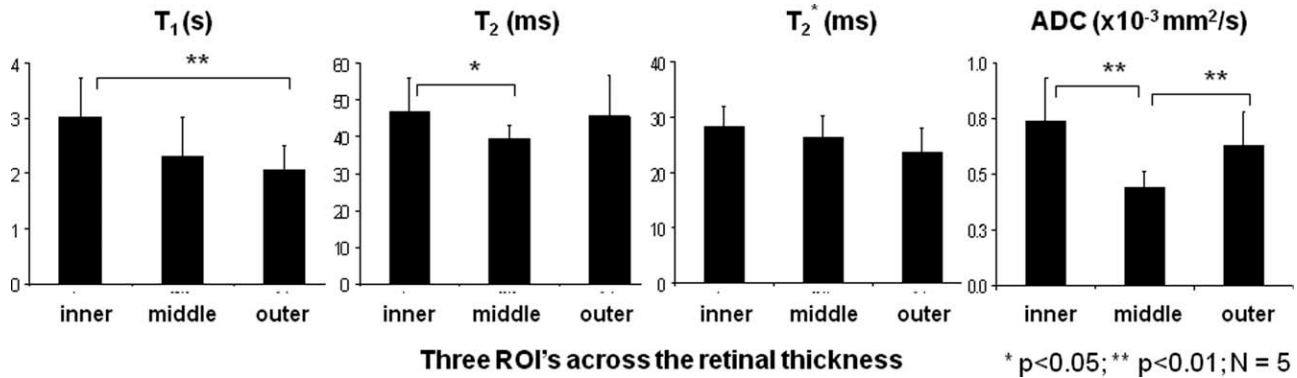


Figure 3. T_1 , T_2 , T_2^* and ADC of three equal layers of the retina. Error bars are standard deviations ($N = 5$ for T_1 , T_2 , and ADC, $N = 4$ for T_2^*).

acquisition (Chen et al., 2008). These results are in good agreement, if the field dependent effect is taken into consideration. By comparison, rat brain T_2 was 47.8 ms at 7 T (Cremillieux et al., 1998).

C. T_2^* . Rat vitreous and whole-retina T_2^* values were, respectively, 55 ± 10 ms and 26 ± 4 ms at 7 T. T_2^* of the retina were shorter than T_2 as expected. We did not find any published report of retinal T_2^* . By comparison, rat brain T_2^* was ~ 30 ms at 7 T (unpublished data).

D. ADC. ADC of the vitreous was $2.3 \pm 0.4 \times 10^{-3}$ mm²/s in this study, 2.7×10^{-3} mm²/s in cat (Shen et al., 2006) and 2.7×10^{-3} mm²/s in mouse (Chen et al., 2008). ADC of the retina was $0.6 \pm 0.2 \times 10^{-3}$ mm²/s in this study, $0.67\text{--}1.2 \times 10^{-3}$ mm²/s (inner two bands) in cat (Shen et al., 2006) and 0.5×10^{-3} mm²/s in mouse (Chen et al., 2008). ADC is magnetic field independent and these results are in good agreement across laboratories and species. By comparison, the whole rat brain ADC range from 0.7×10^{-3} mm²/s to 1.0×10^{-3} mm²/s.

E. Implications for Retinal MRI. Quantitative T_1 , T_2 , T_2^* and ADC could help to optimize anatomical, physiological and functional contrast. Inversion-recovery T_1 -weighted suppression of the vitreous for visual-evoked fMRI studies of the retina has been reported (Duong et al., 2002). Knowledge of the T_1 of the retina

and ocular tissue could help to optimize these T_1 -based MRI studies.

Blood-oxygenation-level-dependent fMRI of the retina would benefit from knowledge of the T_2 and T_2^* relaxation time data. The MRI signal intensity change due to a change in deoxy-hemoglobin concentration has been widely used to detect increased neural activity. Spin-echo BOLD fMRI of the retina has been reported (Cheng et al., 2006). T_2 and T_2^* data of the retina and ocular tissue can be used to improve contrast and sensitivity as well as BOLD fMRI responses in the retina.

ADC of the retina is expected to change in diseases like ischemia and may be a good early and quantitative indicator of the disease process. Furthermore, ADC of the vitreous is markedly higher than that of the retina and an optimized diffusion-weighted imaging could be used to suppress the strong and fast-diffusing vitreous signal. Indeed diffusion-weighted BOLD fMRI has been used to differentially suppress vitreous signal to improve detection of the BOLD fMRI responses in the rat retinas (Cheng et al., 2006).

V. CONCLUSION

This study reports quantitative measurements of water T_1 , T_2 , T_2^* and ADC values of the retina across the retinal thickness at 7 T. Although the spatial resolution is high, PVE of the thin retina of both in-plane resolution and slice thickness could affect the reported quantitative MRI parameters. Current retinal MRI studies chose one or a few central slices to minimize PVE from the retinal

Table I. Comparison of quantitative MRI parameters among rat, cat and mouse retina and brain at different magnetic field strengths.

	Vitreous			Retina			Brain		
	Rat (7 T)	Cat (4.7 T) ^a	Mouse (11.7 T) ^b	Rat (7 T)	Cat (4.7 T) ^a	Mouse (11.7 T) ^b	Rat (7 T)	Cat (4.7 T)	Mouse (11.7 T)
T_1 (s)	4.6 ± 0.5	na	4.2	2.0 ± 0.7	na	2.2	$1.8^{c,d}$	1.5^e	$1.8\text{--}2.3^f$
T_2 (ms)	420 ± 40	218	70	43 ± 9	67, 48, 95 ^g	25	$42\text{--}48^{c,h}$	54^e	$27\text{--}39^f$
T_2^* (ms)	55 ± 10	na	na	26 ± 4	na	na	$20\text{--}25^i$	$25\text{--}30^e$	na
ADC ($\times 10^{-3}$ mm ² /s)	2.3 ± 0.4	2.7	2.7	0.6 ± 0.2	//: 1.1, 1.2, 3.3 ^g ⊥: 0.74, 0.67, 1.2 ^g	0.5		$0.7\text{--}0.9$	

^a Shen et al., 2006.

^b Chen et al., 2008.

^c Guilfoyle et al., 2003.

^d Barbier et al., 2005.

^e Unpublished data.

^f de Graaf et al., 2006.

^g The three values indicate inner, middle and outer strip from cat retina. The inner strip is closest to the vitreous and may be affected by PVE—Shen et al., 2006.

^h Cremillieux et al., 1998.

ⁱ Unpublished data ($n = 7$).

curvature. Future studies may utilize radially positioned slices that are perpendicular to the retinal surface to minimize PVE. Although quantitative MRI parameters have poorer contrasts compared to weighted images and take longer to acquire, quantitative MRI have important values, and, particularly, when comparisons across experimental groups are needed.

REFERENCES

- E.L. Barbier, L. Liu, E. Grillon, J.F. Payen, J. F. Lebas, C. Segebarth, C. Rémy, Focal brain ischemia in rat: Acute changes in brain tissue T_1 reflect acute increase in brain tissue water content, *NMR Biomed* 18 (2005), 499–506.
- B.A. Berkowitz, R. Roberts, J.S. Penn, and M. Gradianu, High-resolution manganese-enhanced MRI of experimental retinopathy of prematurity, *Invest Ophthalmol Vis Sci* 48 (2007), 4733–4740.
- H. Cheng, and T.Q. Duong, Simplified laser-speckle-imaging analysis method and its application to retinal blood flow imaging, *Opt Lett* 32 (2007), 2188–2190.
- H. Cheng, G. Nair, T.A. Walker, M. Kim, M.T. Pardue, P.M. Thule, D.E. Olson, T.Q. Duong, Structural and functional MRI reveals multiple retinal layers, *Proc Natl Acad Sci USA* 103 (2006), 17525–17530.
- K. Cheng, R.A. Waggoner, and K. Tanaka, Human ocular dominance columns as revealed by high-field functional magnetic resonance imaging, *Neuron* 32 (2001), 359–397.
- J. Chen, Q. Wang, H. Zhang, X. Yang, J. Wang, B.A. Berkowitz, S.A. Wickline, S.K. Song, In vivo quantification of T_1 , T_2 , and apparent diffusion coefficient in the mouse retina at 11.74 T, *Magn Reson Med* 59 (2008), 731–738.
- Y. Cremillieux, S. Ding, and J.F. Dunn, High-resolution in vivo measurements of transverse relaxation times in rats at 7 Tesla, *Magn Reson Med* 39 (1998), 285–290.
- R.A. de Graaf, P.B. Brown, S. McIntyre, T.W. Nixon, K.L. Behar, and D.L. Rothman, High magnetic field water and metabolite proton T_1 and T_2 relaxation in rat brain in vivo, *Magn Reson Med* 56 (2006), 386–394.
- T.Q. Duong, and E.R. Muir, Magnetic resonance imaging of the retina, *Jpn J Ophthalmol* 53 (2009), 352–367.
- T.Q. Duong, S.C. Ngan, K. Ugurbil, and S.G. Kim, Functional magnetic resonance imaging of the retina, *Invest Ophthalmol Vis Sci* 43 (2002), 1176–1181.
- T.Q. Duong, D.-S. Kim, K. Ugurbil, S.-G. Kim, Localized blood flow response at sub-millimeter columnar resolution, *Proc Nat Acad Sci* 98 (2001), 10904–10909.
- J.G. Fujimoto, C. Pitris, S.A. Boppart, and M.E. Brezinski, Optical coherence tomography: An emerging technology for biomedical imaging and optical biopsy, *Neoplasia* 2 (2000), 9–25.
- D.N. Guilfoyle, V.V. Dyakin, J. O’ shea, G.S. Pell, and J.A. Helpert, Quantitative measurements of proton spin-lattice (T_1) and spin-spin (T_2) relaxation times in the mouse brain at 7.0 T, *Magn Reson Med* 49 (2003), 576–580.
- D.R. Guyer, L.A. Yannuzzi, J.S. Slakter, J.A. Sorenson, and S. Orlock, The status of indocyanine-green videoangiography, *Cur Opin Ophthalmol* 4 (1993), 3–6.
- D.-S. Kim, T.Q. Duong, S. -G. Kim, High-resolution mapping of iso-orientation columns by fMRI, *Nat Neurosci* 3 (2000), 164–169.
- Y. Li, H. Cheng, and T.Q. Duong, Blood-flow magnetic resonance imaging of the retina, *Neuroimage* 39 (2008), 1744–1751.
- D.A. Nelson, S. Krupsky, A. Pollack, E. Aloni, M. Belkin, I. Vanzetta, M. Rosner, A. Grinvald, Special report: Noninvasive multi-parameter functional optical imaging of the eye, *Ophthalmic. Surg Lasers Imaging* 36 (2005), 57–66.
- P.R. Preussner, G. Richard, O. Darrelmann, J. Weber, and I. Kreissig, Quantitative measurement of retinal blood flow in human beings by application of digital image-processing methods to television fluorescein angiograms, *Graefes Arch Clin Exp Ophthalmol* 221 (1983), 110–112.
- C.E. Riva, S.D. Cranstoun, R.M. Mann, and G.E. Barnes, Local choroidal blood flow in the cat by laser Doppler flowmetry, *Invest Ophthalmol Vis Sci* 35 (1994), 608–618.
- A.C. Silva, and A.P. Koretsky, Laminar specificity of functional MRI onset times during somatosensory stimulation in rat, *Proc Natl Acad Sci USA* 99 (2002), 15182–15187.
- Q. Shen, H. Cheng, M.T. Pardue, T.F. Chang, G. Nair, V.T. Vo, R.D. Shonk, T.Q. Duong, Magnetic resonance imaging of tissue and vascular layers in the cat retina, *J Magn Reson Imaging* 23 (2006), 465–472.